ACS EARTH AND SPACE CHEMISTRY

http://pubs.acs.org/journal/aesccq

Article

Influence of Ammonia and Relative Humidity on the Formation and Composition of Secondary Brown Carbon from Oxidation of 1-Methylnaphthalene and Longifolene

Yumeng Cui, Alexander L. Frie, Justin H. Dingle, Stephen Zimmerman, Isis Frausto-Vicencio, Francesca Hopkins, and Roya Bahreini*

Cite This: https://doi.org/10.1021/acsearthspacechem.0c00353

Read Online

ACCESS | Metrics & More | Article Recommendations | Supporting Information

ABSTRACT: Improved understanding of the optical properties of secondary organic aerosol (SOA) particles is needed to better predict their climate impacts. Here, SOA was produced by reacting 1-methylnaphthalene or longifolene with hydroxyl radicals (OH) under variable ammonia (NH_3), nitrogen oxide (NO_x), and relative humidity (RH) conditions. In the presence of NH_3 and NO_x, longifolene-derived aerosols had relatively high single scattering albedo (SSA) values and low absorption coefficients at 375 nm independent of RH, suggesting that the longifolene SOA is mostly scattering. In 1-methylnaphthalene experiments, the resulting SSA and SOA mass absorption coefficient (MAC_{org}) values suggest the formation of light-absorbing SOA, and the addition of high NO_x and high NH_3 enhanced the SOA absorption. Under intermediate-NO_x dry conditions, the MAC_{org} values increased from 0.13 $m^2\ g^{-1}$ in NH_3-free conditions to 0.28 $m^2\ g^{-1}$ in high-NH_3 conditions. Under high-NH_3 conditions, the MAC_{org} value further increased to 0.36 $m^2\ g^{-1}$ with an increase in RH. Under dry high-NO_x conditions, the MAC_{org} value increased from 0.42 to 0.67 $m^2\ g^{-1}$ with the addition of NH_3, while with elevated RH, the MAC_{org} value reached 0.70 $m^2\ g^{-1}$. The time series of MAC_{org} showed increasing trends only in the presence of NH_3. Composition analysis of SOA suggests that organonitrates, nitroorganics, and other nitrogen-containing organic compounds (NOCs) are potential chromophores in the 1-methylnaphthalene SOA. Significant formation of NOCs was observed in the presence of high-NO_x and NH_3 and was enhanced under elevated RH.

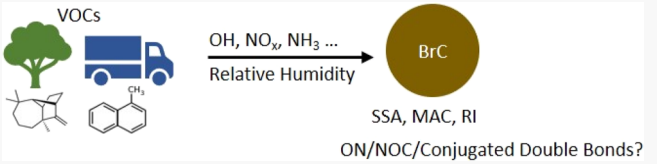

KEYWORDS: *secondary organic aerosol, brown carbon, ammonia, oxidized and reduced nitrogen-containing compounds, refractive index*

1. INTRODUCTION

Atmospheric aerosols play an important role in controlling the Earth's radiative balance by directly and indirectly interacting with solar radiation. The Intergovernmental Panel on Climate Change Fifth Assessment Report (IPCC AR5) suggested that the average global climate forcing values from black carbon (BC) and organic carbon emitted directly from sources like biomass burning and fossil fuel combustion are +0.64 W m^{-2} (+0.25 to +1.1 W m^{-2}) and −0.29 W m^{-2} (−0.5 to −0.09 W m^{-2}), respectively.[1] However, the estimation of radiative forcing for secondary organic aerosols (SOAs) was not included in IPCC AR5 because formation pathways and the physical and chemical properties of SOA are currently poorly understood. Although the distribution and relative concentration of SOA in the atmosphere vary among regions, Hallquist et al. estimated that globally 70−90% of organic aerosol (OA) is SOA, which is produced from atmospheric multi-phase reactions.[2]

Recent studies have shown that light-absorbing organic compounds, known as brown carbon (BrC), could be emitted directly together with BC from biomass burning and fossil fuel combustion or formed secondarily as SOA in the atmosphere.[3−5] BrC can absorb solar radiation strongly in the visible to near-ultraviolet (near-UV) range.[3,6−8] Despite more research being carried out in recent years using field measurements and chamber studies of BrC, the chemical and optical properties of secondary BrC are still highly uncertain.[4] The large uncertainties in radiative forcing estimates of secondary BrC decrease the certainty of current climate model projections. Wang et al. estimated a global mean top-of-the-atmosphere direct refractive effect of +0.48 W m^{-2} for BrC,[9] suggesting an overall global warming effect by BrC. Many recent studies that focused on the chemical and optical properties of lab-generated and ambient BrC suggest that conjugated systems,[10−12] organonitrate and nitroorganic groups,[12−15] and reduced nitrogen-containing organic compounds (NOCs)[16−20] in BrC could act as strong light-

Received: December 28, 2020
Revised: March 25, 2021
Accepted: March 26, 2021

Table 1. Summary of Experiments[a]

VOC	hydroxyl radical source	[b]HC_0 (ppbv)	[c]ΔHC (ppbv)	[d]$NO_{x,0}$ (ppbv)	[e]$[HC/NO_x]_0$	[f]$NH_{3,0}$ (ppbv)	[g]RH (%)	ρ_{eff} (g/cc)	[h]$RI_{org,100min}$ $n^{+0.09}_{-0.07}$	[h]$RI_{org,100min}$ $k^{+0.006}_{-0.004}$	plot reference
Lgf	HONO	80	80	550	0.1	180	5	1.13 ± 0.007	1.36	0.001	I
Lgf	HONO	70	70	550	0.1	200	10	1.13 ± 0.007	1.36	0.001	II
Lgf	HONO	100	100	740	0.1	130	45	1.16 ± 0.04	1.37	0.001	III
Lgf	HONO	90	90	550	0.2	180	45	1.16 ± 0.04	1.38	0.002	IV
1-MN	H_2O_2	160	60	5	32	170	10	1.12 ± 0.03	1.46	0.007	I
1-MN	H_2O_2	140	75	5	28	120	10	1.12 ± 0.03	1.44	0.007	II
1-MN	H_2O_2	60	50	10	4	<5	5	1.52 ± 0.03	1.48	0.004	III
1-MN	H_2O_2	75	45	5	19	<5	5	1.52 ± 0.03	1.48	0.005	IV
1-MN	H_2O_2	170	70	10	17	260	40	1.18 ± 0.03	1.47	0.011	V
1-MN	HONO	75	30	520	0.1	190	5	1.18 ± 0.05	1.31	0.020	VI
1-MN	HONO	315	105	880	0.3	<5	15	1.31 ± 0.08	1.57	0.015	VII
1-MN	HONO	240	100	720	0.3	<5	20	1.31 ± 0.08	1.56	0.017	VIII
1-MN	HONO	160	80	440	0.4	210	40	1.26 ± 0.07	1.45	0.024	IX
1-MN	HONO	160	50	350	0.5	170	40	1.26 ± 0.07	1.46	0.026	X

[a]Lgf = longifolene, 1-MN = 1-methylnaphthalene. [b]HC_0 is based on the initial conditions measured at the beginning of the photooxidation reactions. [c]ΔHC is the reacted hydrocarbon concentration by the end of the photooxidation experiments. For longifolene experiments, the hydrocarbon concentrations were below the GC−FID detection limit toward the end of the experiment, so we assume that there was no gas-phase longifolene in the chamber at the end of the experiments. [d]$NO_{x,0}$ is based on the initial conditions measured at the beginning of the photooxidation reactions. [e]$[HC/NO_x]_0$ is the initial hydrocarbon-to-NO_x ratio. [f]$NH_{3,0}$ is based on the initial conditions measured at the beginning of the photooxidation reactions. [g]RH values are based on the average RH measured by the RH probe during the photooxidation reactions. [h]$RI_{org,100min}$ are derived only for the organic components of the aerosol at 100 min after irradiation or at the end of the experiment if the reaction time was less than 100 min.

absorbing chromophores and are responsible for the absorption of tropospheric solar radiation. The extent of browning and the optical properties of the resulting SOA vary greatly among SOA from different precursors and oxidants and further changes with aging under different conditions.[4,21−27]

Lambe et al. suggested the importance of light-absorbing components by conjugated double bonds retained in the oxidation products of aromatic precursors that can extend SOA absorption toward longer wavelength in the UV−visible range.[10] Jacobson suggested that nitroaromatic gases and nitrated and aromatic aerosols contributed for 25−30% of the reduction in UV irradiance within the boundary layer in the Los Angeles Basin area.[28] A more recent study showed that SOA formation from anthropogenic volatile organic compounds (VOCs) is the major source of water-soluble BrC in the Los Angeles Basin, and light absorption from water-soluble nitroaromatics was identified to contribute up to 3.8% of the observed ambient near-UV to UV absorption.[29] Lab-generated SOA formed under high-NO_x conditions also indicated that organonitrates and nitroorganics are important components in aromatic SOA,[30] absorbing near-UV to UV light.[3,27,29,31] In addition to the studies on the effect from NO_x, there are some studies focused on the effect of NH_3/NH_4^+ on the optical properties of SOA. SOA produced by O_3-initiated limonene oxidation became brown after exposure to reduced nitrogen compounds including NH_3, NH_4^+, and amino acids.[32] The optical measurements as well as chemical composition measurements suggest that the newly formed light-absorbing moieties were likely to be conjugated nitrogen-containing organic species.[18,32,33] Bones et al. and Laskin et al. suggested that this kind of browning involving reduced nitrogen compounds was induced by condensation reactions between NH_3/NH_4^+ and carbonyls, which produces the light-absorbing imine (C═N) bond.[32,33] Huang et al. and Qi et al. carried out chamber experiments to explore the aromatic SOA formation in the presence of gas-phase NH_3 and observed the formation of NOCs in the particle phase, which significantly increased the resulting SOA absorption.[34,35] In addition to the reaction with carbonyls, NH_3 can also react with organic and inorganic acids forming particle-phase ammonium salts.[36,37] Chen et al. suggested that the addition of NH_3 enhanced the formation of secondary aerosol from the photooxidation of gasoline vapor due to the formation of inorganic NH_4NO_3 and NOCs.[38]

Relative humidity (RH) can also play a role in SOA formation and composition,[39] thus affecting its optical properties. For example, water vapor can react with hydrocarbon oxidation products in the gas phase or suppress aerosol-phase condensation reactions that produce water molecules.[40,41] Furthermore, RH was shown to control aerosol uptake of NH_3 by influencing the aerosol water content and therefore viscosity and molecular diffusion in aerosols.[42,43] Lian et al. observed the formation of imidazole compounds from the reaction between carbonyls and ammonium/amines in ambient aerosols and provided evidence that cloud processing could enhance the formation of particulate imidazole.[44] Additionally, aqueous-phase hydrolysis reactions may lead to loss of organonitrates,[45,46] thus affecting the absorption characteristics of BrC. There is limited research focused on the effect of NH_3 on optical and chemical properties of SOA under atmospherically relevant RH.

In this study, we examined the optical and chemical properties of SOA formed from photooxidation of a biogenic hydrocarbon (longifolene) and an anthropogenic polycyclic aromatic hydrocarbon (PAH) (1-methylnaphthalene) (1-MN) in a Teflon chamber under variable levels of NO_x, NH_3, and RH. The selected compounds are representative compounds in their class with a relatively high SOA formation potential.[30,47,48] Longifolene is a tricyclic sesquiterpene, which is found predominantly in pine resins.[49] Longifolene is an important precursor to atmospheric aerosols due to its high reactivity with hydroxy radicals (OH) and nitrate radicals (NO_3) and high SOA yields.[47,49,50] 1-MN is a PAH which is a

https://doi.org/10.1021/acsearthspacechem.0c00353
ACS Earth Space Chem. XXXX, XXX, XXX−XXX

commonly found anthropogenic hydrocarbon in the polluted environment. 1-MN and OH-initiated photooxidation reactions result in relatively high SOA formation.[30] Previous work investigated 1-MN SOA formation in a variety of NO_x regimes and found that the chemical and physical properties of 1-MN SOA were significantly impacted by NO_x conditions.[30,48,51] We hypothesize that, in the presence of NH_3, the SOA formed from these VOCs contains chromophores which could significantly enhance SOA absorption. On-line chemical and microphysical measurements of aerosols were performed during chamber experiments, and aerosols' single scattering albedo (SSA), SOA mass absorption coefficient (MAC_{org}), and refractive index (RI_{org}) were determined in each experiment. Evolution in the chemical and optical properties was also evaluated to identify the formation of possible chromophores in the resulting SOA. Our results indicate that the longifolene SOA remained as mostly scattering under high-NO_x and high-NH_3 conditions regardless of RH. On the other hand, organonitrates and/or nitroorganics and other NOCs were important chromophores in 1-MN SOA, and the formation of NOCs was promoted under higher RH.

2. METHODS

2.1. Chamber Experiments and Instrumentation. A detailed description of the chamber experimental setup and instrumentation used in this work can be found in Dingle et al.[51] Essentially, the chamber is a 1.5−2.0 m^3 PFA Teflon bag in a metallic frame enclosure. The initial RH in the chamber was adjusted by injecting dry zero air and water vapor for different experiments resulting in average RH 40−45% for humid experiments and <20% for dry experiments. The OH sources for photooxidation experiments were hydrogen peroxide (H_2O_2, for intermediate-NO_x experiments) or nitrous acid (HONO, for high-NO_x experiments). The resulting average concentrations of OH from the above sources in the chamber were calculated as 6.3×10^6 and 3.6×10^7 molecules cm^{-3}, respectively.[51] Details of these estimations are presented in the Supporting Information. For high-NO_x experiments, we injected additional NO to achieve the initial NO_x concentrations of ∼500 ppbv. Although for intermediate-NO_x experiments we did not inject any additional NO or NO_2, trace amounts of NO_x from zero air introduced in the chamber led to the initial NO_x concentration in these experiments to be ∼3−15 ppbv. In addition to NO, we injected NH_3 in some experiments before the initiation of irradiation to create a high-NH_3 condition (∼120−260 ppbv). Table 1 shows the summary of experimental conditions used in this work. Four of the experiments described by Dingle et al. are also presented in the following section for comparison with the high-NH_3 experiments and to better illustrate the influence of NH_3 on the chemical and optical properties of SOA.[51]

Once the gas-phase concentration of the parent hydrocarbon was stable in the chamber, irradiation by UV lights initiated photooxidation. A significant amount of SOA particles (with maximum volume concentration ≈30−95 μm^3 cm^{-3} under different experimental conditions) from VOCs (longifolene or 1-MN) were generated by nucleation and condensation (Figure S1).

In this work, we used a diverse set of instruments measuring both gas-phase and particle-phase compounds. A gas chromatograph coupled with a flame ionizing detector (GC−FID, Hewlett Packard 5890 Series II) was used for measuring the concentrations of the injected VOCs. A UV photometric ozone analyzer (Thermo, model 49i) and a chemiluminescence NO−NO_2−NO_x analyzer (Thermo, model 42i) were used to measure gas-phase ozone and NO−NO_2−NO_x concentrations at 1 Hz. We also used a cavity ring-down spectrometer (Picarro G2123) to monitor the NH_3 concentration in the chamber during the high-NH_3 experiments.

For particle-phase measurements, various instruments sampled air from the chamber through a 30 cm-long diffusion dryer containing silica gel (Sigma-Aldrich, Saint Louis, MO, USA) and Purafil (Thermo Scientific). A scanning electrical mobility spectrometer (SEMS, Brechtel Manufacturing Inc.) was used to measure the number concentration and size distribution of particles in the range of 10−740 nm. Based on the calibration with polystyrene latex sphere standards, the sizing accuracy of SEMS was determined to be ∼±4%. A photoacoustic extinctiometer (PAX, Droplet Measurement Technology) measured aerosol's scattering and absorption coefficient at 375 nm at 1 Hz ($\beta_{scat,375}$ and $\beta_{abs,375}$); the detection limits defined as 2 times the standard deviation of scattering and absorption coefficients of filtered air averaged to SEMS time (140 s) were ∼1.9 and ∼2.1 M m^{-1} for $\beta_{scat,375}$ and $\beta_{abs,375}$, respectively. Total mass and size-dependent chemical composition of SOA particles were measured at 15 s intervals using a mini-aerosol mass spectrometer (mAMS) coupled with a compact time-of-flight (ToF) mass spectrometer (Aerodyne Research). The mass accuracy of the mAMS was determined to be ±20 ppm and the resolving power was ∼1200−1300. The relatively high ionization energy and vaporization temperature within the mAMS fragmented the aerosols into small ions; thus, tracers of chemical composition information are provided as mass concentration of specific ions at specific mass-to-charge ratios (m/z).[52] Several fragments (m/z = 44, CO_2^+, m/z = 43, $C_2H_3O^+$) are often used as important indicators of chemical composition and aging of oxygenated SOA.[53,54] The m/z = 27 (CHN^+), m/z = 30 (NO^+, CH_4N^+), m/z = 46 (NO_2^+), m/z = 40 ($C_2H_2N^+$), and m/z = 76 ($C_6H_4^+$) are also considered for the SOA composition in this study.[30,38,55] The mAMS data were analyzed by high-resolution (HR)-ToF-AMS analysis toolkit 1.61B and PIKA module for SQUIRREL 1.21B.

2.2. SSA, MAC, and RI Calculations. The SSA of aerosols at 375 nm was determined with $\beta_{scat,375}$ and $\beta_{abs,375}$ measured by PAX using eq 1.[56,57]

$$SSA_{375} = \frac{\beta_{scat,375}}{\beta_{scat,375} + \beta_{abs,375}} \quad (1)$$

Aerosols' SSA is size dependent; thus, we explored its dynamics as a function of size parameter (α). α was determined by aerosol electrical mobility diameter (d_m) representing the mode of the size distributions measured by SEMS and the wavelength of radiation used in PAX (λ = 375 nm) as eq 2.[58]

$$\alpha_{375} = \frac{\pi d_m}{\lambda} \quad (2)$$

The relative uncertainties of the calculated SSA were determined by propagating the errors in $\beta_{scat,375}$ and $\beta_{abs,375}$ and were determined to be ∼2−9% in different experiments.

MAC at 375 nm was calculated using the organic mass concentration of the aerosols (M_{OA}) (detailed description given in the Supporting Information) and $\beta_{abs,375}$ obtained from PAX using eq 3.[59] Relative uncertainties of MAC_{org} were

https://doi.org/10.1021/acsearthspacechem.0c00353
ACS Earth Space Chem. XXXX, XXX, XXX−XXX

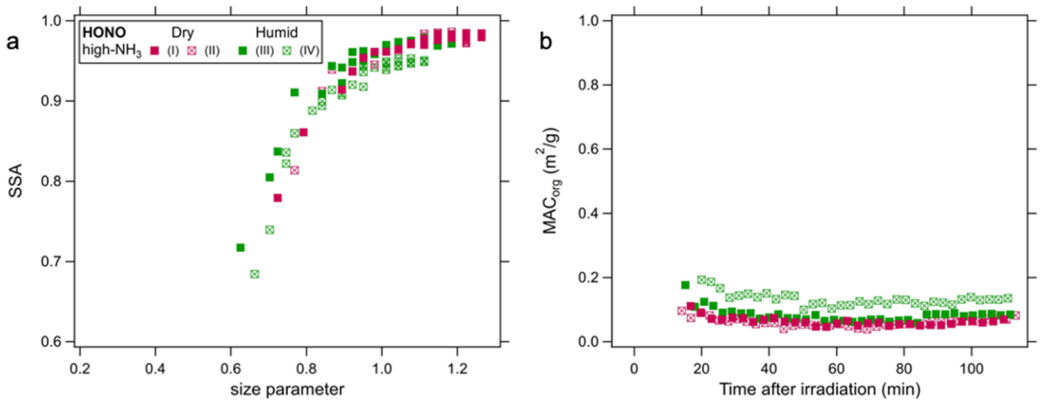

Figure 1. (a) SSA vs size parameter at 375 nm and (b) MAC_{org} vs photooxidation reactions time for longifolene-derived aerosol particles. All longifolene experiments were done under high-NO_x, high-NH_3 conditions; the pink markers refer to the experiments under dry conditions; the green markers refer to the experiments under humid conditions. Open and closed markers represent the duplicate runs of the same condition.

determined by propagating errors in $\beta_{abs,375}$ and mass of organic components in aerosols and were ~6−16% in different experiments.

$$MAC_{org} = \frac{\beta_{abs,375}}{M_{OA}} \quad (3)$$

Aerosol effective densities were determined by comparing parallel AMS aerosol mass distributions and SEMS volume distributions.[60,61] AMS mass distributions are measured versus the vacuum aerodynamic diameter (d_{va}) while SEMS volume distributions are a function of electrical mobility diameter (d_m). Assuming particle sphericity, the effective density was determined as follows

$$\rho_{eff} = \frac{d_{va}}{d_m}\rho_0 \quad (4)$$

where ρ_0 is the unit density (1 g cm^{-3}). The calculated effective densities are listed in Table 1.

RI is an indicator of the interaction between the material and radiation. RI values were calculated based on Mie theory and by an optical closure procedure.[26,62,63] The aerosols did not show any size-dependent composition difference (Figure S2); thus, we assumed that the aerosols were homogeneous and internally mixed and applied Mie theory to our system. Basically, the theoretical $\beta_{scat,375,theo}$ and $\beta_{abs,375,theo}$ were calculated with a broad range of n (1.3−1.8) and k (0−0.05) values and at small increments (0.01 for n and 0.001 for k) using the measured size distribution.[63] The n and k pair that resulted in the best match of the calculated values of $\beta_{scat,375,theo}$ and $\beta_{abs,375,theo}$ with the measured $\beta_{scat,375}$ and $\beta_{abs,375}$ by minimizing the merit parameter Δ (defined by eq 5) were assigned as aerosol's n and k.[14]

$$\Delta = |(\beta_{scat,375} - \beta_{scat,375,theo})| + |(\beta_{abs,375} - \beta_{abs,375,theo})| \quad (5)$$

The aerosol RI contains the contribution from both inorganic and organic species in the particle phase. The following equations were used to derive the RI of pure organic compounds in the aerosol (n_{org} and k_{org}), assuming well-mixed particles and volume weighting of the RI of the mixture components.[64,65] The relative uncertainties in n and k values were determined by the uncertainties in measured $\beta_{scat,375}$ and $\beta_{abs,375}$ and size distribution uncertainties.

$$n = n_{inorg} \times VF_{inorg} + n_{org} \times VF_{org} \quad (6)$$

$$k = k_{inorg} \times VF_{inorg} + k_{org} \times VF_{org} \quad (7)$$

where n_{inorg} and k_{inorg} are the RI values of NH_4NO_3 and HNO_3 and VF_{inorg} and VF_{org} are the volume fractions of the inorganic and organic components in the aerosols, respectively. The relative uncertainties in n_{org} and k_{org} values were determined by the uncertainties in n and k values, VF_{inorg} and VF_{org}, and the overall uncertainties are listed in Table 1. Details of these calculations are provided in the Supporting Information.

The derived n_{org} and k_{org} values at the end of the experiments, final SSA of aerosols, and MAC_{org} values at ~100 min of oxidation time along with their corresponding uncertainties are listed in Tables 1 and S1. Since aerosol particles nucleated and grew very fast at the initial stages of oxidation, SEMS could not capture the true size distribution during this time because of its relatively long scan time (140 s), so we present the corresponding measurements when the aerosol mode increased by less than 10% between two consecutive SEMS runs.

Given the short photooxidation reaction times in our system, we do not expect particle wall loss to be significant. Furthermore, the presented results on SSA and RI are based on aerosols' intensive properties. Therefore, wall loss correction has not been applied to the data.

2.3. Organonitrate and Nitroorganic Fraction Calculation. Fractional contribution of $-ONO_2$ (organonitrate) and $-NO_2$ (nitroorganic) functional groups to total organic matter in particle phase was calculated in each experiment. Due to the fragmentation by mAMS, our analysis cannot distinguish between the organonitrate and nitroorganic groups; thus, here we calculated the total fraction of organic nitrate ($NO_{x}^{+}{}_{org}$) from these two groups to the measured organics. First, we calculated the fractional contribution of $NO_{x}^{+}{}_{org}$ ions to total NO_3^- as follows.[55]

$$x = \frac{(R_{obs} - R_{AN})(1 + R_{lit})}{(R_{lit} - R_{AN})(1 + R_{obs})} \quad (8)$$

where R_{obs} is the observed $[NO^+]/[NO_2^+]$ in the experiments from mAMS analysis, R_{lit} is the literature value of $[NO^+]/[NO_2^+]$ from $NO_{x}^{+}{}_{org}$ (assumed as 10),[66] and R_{AN} is the calculated $[NO^+]/[NO_2^+]$ value from mAMS NH_4NO_3 calibration, representing the inorganic nitrate contribution to NO_3^-.[55,67] Calculations were repeated with R_{lit} = 5 and 15 to

https://doi.org/10.1021/acsearthspacechem.0c00353
ACS Earth Space Chem. XXXX, XXX, XXX−XXX

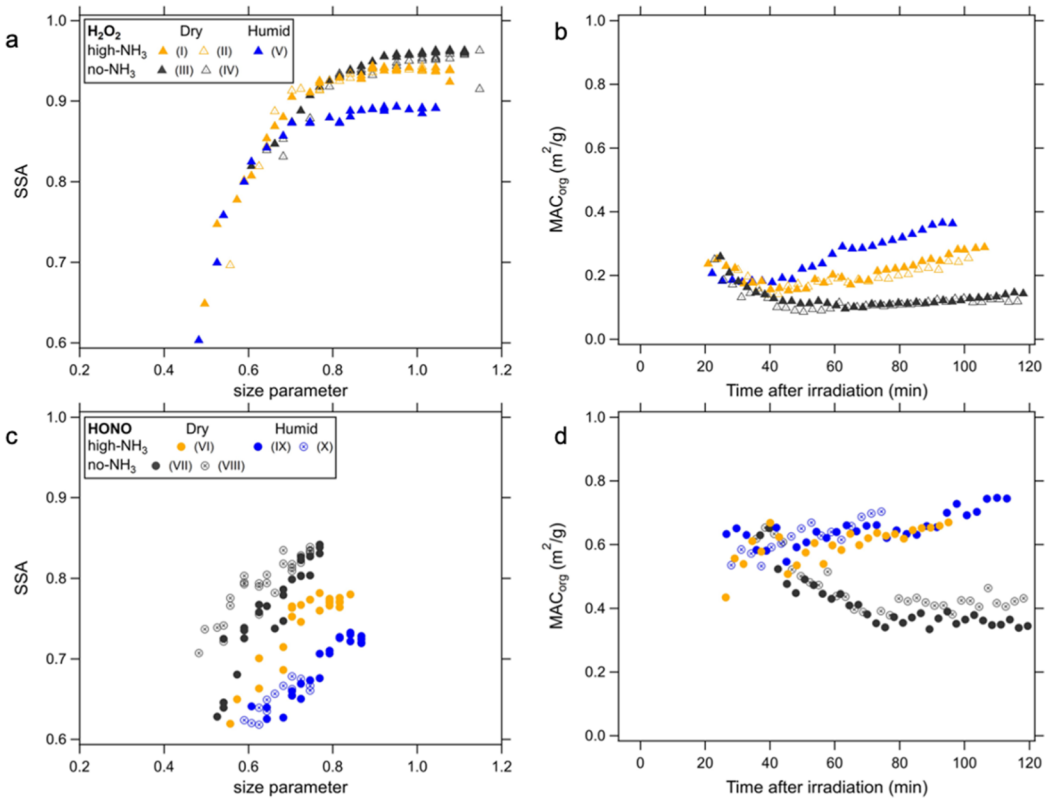

Figure 2. (a) SSA vs size parameter at 375 nm and (b) MAC_{org} vs photooxidation reactions time for 1-MN-derived aerosols under intermediate-NO_x conditions; (c) SSA vs size parameter at 375 nm, and (d) MAC_{org} vs photooxidation reactions time for 1-MN-derived aerosols under high-NO_x conditions. The gray markers refer to the experiments under no-NH_3, dry conditions; the yellow markers refer to the high-NH_3, dry experiments and the blue markers refer to the high-NH_3, humid experiments. Open and closed markers represent the duplicate runs of the same condition.

bound the uncertainties for RI_{org} and MAC_{org} estimations. We then calculated the ratio of $NO_x^+{}_{org}$ to measured organics as follows.

$$R_{ON} = x\frac{[NO_3^-]}{[OA]} \quad (9)$$

where $[NO_3^-]$ is the mass concentration of nitrate (both organic and inorganic) and [OA] is the mass concentration of OAs measured by mAMS during the experiments.

3. RESULTS AND DISCUSSION

3.1. Longifolene SOA with HONO as an Oxidant. In longifolene experiments, particle volume and mass concentrations increased at a fast rate after the initiation of oxidation and reached peak values after 1 h. β_{scat} also showed a similar trend as the experiments went on, while β_{abs} remained low and almost constant regardless of RH. The profiles of SSA and MAC_{org} during longifolene experiments are shown in Figure 1. The SSA is shown as a function of size parameter at 375 nm. The SSA in the presence and absence of NH_3 remained very high at larger aerosol sizes (with SSA_{max} = 0.95−1),[51] suggesting that aerosols formed from OH oxidation under high-NO_x conditions were mostly scattering regardless of NH_3 concentration. Additionally, the MAC_{org} values of longifolene SOA (<0.2 m^2 g^{-1}) were significantly lower than the MAC_{org} values from previous studies on absorbing SOA,[4] indicating that the longifolene SOA formed in the current experiments was only weakly absorbing.

3.2. 1-MN SOA with H_2O_2 as an Oxidant Precursor. Both aerosol mass and volume concentrations in 1-MN oxidation by OH (under intermediate-NO_x conditions with H_2O_2 as the OH precursor) increased soon after the irradiation of UV light and reached their peaks after about 70−80 min of oxidation. Compared with longifolene SOA, the β_{abs} values of 1-MN-derived aerosols were higher despite having lower NO_x concentrations, suggesting that 1-MN has a greater potential for forming light-absorbing aerosols in the atmosphere.

3.2.1. Effect of NH_3 under Dry Conditions. As shown in Figure 2a, in dry intermediate-NO_x experiments and in the absence of NH_3, the SSA values increased from 0.8 at a size parameter of 0.6 and stabilized at 0.96 at a size parameter of 0.9. However, similar experiments in the presence of NH_3 resulted in a slightly lower SSA of 0.94 at similar large size parameters. Despite minor changes in SSA and k_{org}, differences in MAC_{org} are significant and beyond the propagated uncertainties in the derivations, suggesting that under dry conditions with intermediate-NO_x, NH_3 has the potential to promote formation of more absorbing 1-MN SOA (for non-NH_3 experiments, MAC_{org} ≈ 0.13 m^2 g^{-1}; for high-NH_3 experiments, MAC_{org} ≈ 0.25−0.28 m^2 g^{-1}). Moreover, in contrast to the experiments without NH_3, MAC_{org} in high-NH_3 experiments showed a significant increase with reaction time, suggesting that NH_3 is the main factor driving the chemistry toward additional formation of absorbing aerosol components and increase of SOA absorption per mass in this system.

To better understand the chemistry driving the differences in the SOA optical properties observed in each experiment, HR

https://doi.org/10.1021/acsearthspacechem.0c00353
ACS Earth Space Chem. XXXX, XXX, XXX−XXX

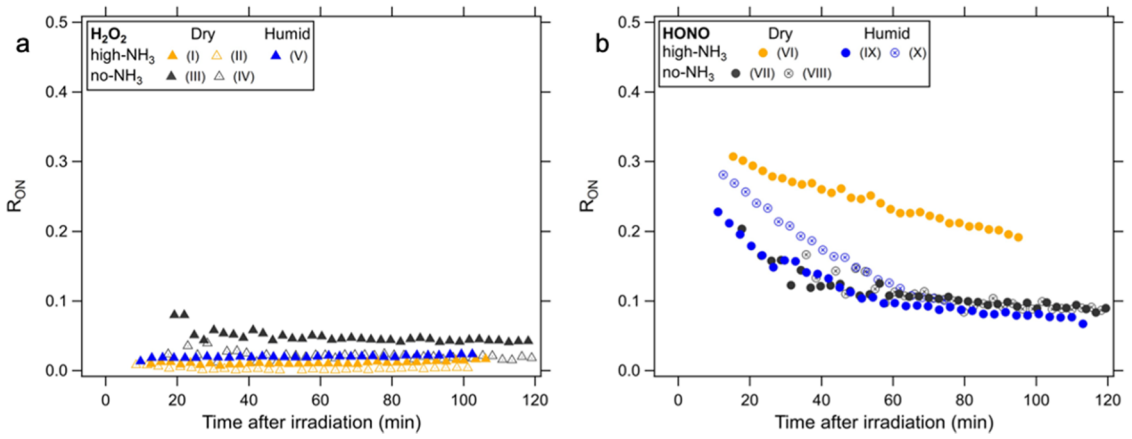

Figure 3. Calculated R_{ON} of 1-MN SOA particles over the course of photooxidation experiments under (a) intermediate-NO_x conditions and (b) high-NO_x conditions. The gray markers refer to the experiments under no-NH_3, dry conditions; the yellow markers refer to the high-NH_3, dry experiments and the blue markers refer to the high-NH_3, humid experiments. Open and closed markers represent the duplicate runs of the same condition.

analyses of the mAMS data were carried out. Carbonyl compounds are one of the major products from OH-initiated 1-MN oxidation reactions.[48,68] Carbonyl groups may react with ammonia and form imine groups.[17,69] These nitrogen-containing compounds may absorb light strongly, especially in the near-UV wavelength range. Thus, in this work, we also focused on identifying the possible light-absorbing NOCs using mAMS HR mass spectra to examine ions that could act as markers for the formation of NOCs and evaluated the contribution of NOCs to total SOA absorption. Under dry conditions and in the presence of NH_3, possibly due to the detection limits of our instruments and relatively low OH exposure values, our analysis show only slightly increased fractions of some nitrogen-containing ions after the addition of NH_3 (Figure S3), including CHN^+, CH_4N^+, and $C_2H_2N^+$. Although we observed the increased fraction of these ions, their relatively low concentration (<0.6% to total aerosol mass) suggests that under the current H_2O_2-initiated experimental conditions, the proposed NH_3−carbonyl reactions may not be able to produce significant NOCs. Nguyen et al. reported that negligible contribution from NOCs (<1%) in limonene SOA after exposure to ammonium sulfate solution drastically enhanced the resulting aerosols' absorption without significant change in overall molecular composition.[18] Whether low concentrations of NOCs contributed to any light absorption in this system remains to be studied in the future with more sensitive instrumentation.

3.2.2. Effect of RH under High-NH_3 Conditions. Under high-NH_3 concentrations, the SSA and MAC_{org} from the dry and humid experiments showed significant differences, indicating that RH is an important factor influencing the optical properties of the resulting aerosols (Figure 2a,b). Under humid and dry conditions, SSA reached maximum values of 0.89 and 0.96, respectively, and MAC_{org} values were 0.36 and 0.28 $m^2\ g^{-1}$ after 100 min of UV irradiation, respectively. As for the RI, n_{org} was 1.44−1.47 under both conditions, while k_{org} reached 0.011 in humid conditions and 0.007 under dry conditions. Additionally, the MAC_{org} value increased at a faster rate under humid conditions (≈0.0032 $m^2\ g^{-1}\ min^{-1}$ compared to dry condition 0.0019 $m^2\ g^{-1}\ min^{-1}$). All these observations lead us to conclude that in the OH-initiated oxidation of 1-MN, higher RH (~40%) strengthens the potential for forming absorbing SOA compared to the experiments under lower RH conditions (<20%).

The calculated R_{ON} from both low and high RH experiments under intermediate-NO_x conditions were low (<5%) (Figure 3a), suggesting that without any additional injections of NO_x, the elevated RH and NH_3 would not influence the formation and fate of organonitrates and/or nitroorganics. Similar to dry experiments, our current analysis did not show any significant signal from NOCs as an indicator of strong chromophore formation under humid conditions in the presence of NH_3 with H_2O_2 as the oxidant source. As discussed above, although we believe that NH_3 was involved in the chemistry and formation of absorbing SOA,[7,17] the formed compounds that increased MAC_{org} (Figure 2b) may be of low concentration or fragment significantly such that our mAMS analysis could not capture their presence.

3.3. 1-MN SOA with HONO as an Oxidant Precursor. Similar to the H_2O_2-initiated oxidation reaction, the aerosol mass and volume concentration increased soon after the start of UV irradiation and reached their peaks after about 1 h of oxidation. However, compared to the H_2O_2 experiments, the aerosol volume concentrations in HONO experiments were significantly lower, possibly due to high concentration of NO_x in HONO experiments, which suppresses SOA formation by favoring the formation of more volatile products.[70,71] The SSA values were lower and the MAC_{org} and k_{org} values were higher under high-NO_x conditions compared to the previously described H_2O_2 experiments, indicating that NO_x has a significant influence on 1-MN SOA optical properties.

3.3.1. Effect of NH_3 under Dry Conditions. Figure 2c,d shows the SSA and MAC_{org} results from HONO experiments. For high-NO_x experiments, SSA in the absence of NH_3 reached 0.85 at a size parameter of 0.84, while at the same size parameter, SSA from the high-NH_3 experiments was significantly lower at approximately 0.78. Additionally, MAC_{org} and RI_{org} results were consistent with the SSA observations (with MAC_{org} ≈ 0.36−0.42 $m^2\ g^{-1}$, n_{org} = 1.57, and k_{org} = 0.015−0.017 in the absence of NH_3; MAC_{org} ≈ 0.67 $m^2\ g^{-1}$, n_{org} = 1.31, and k_{org} = 0.020 with high concentration of NH_3), suggesting that under high-NO_x and dry conditions, NH_3 significantly increases 1-MN SOA absorption. Similar to the observations described before, under high-NO_x condition, the

https://doi.org/10.1021/acsearthspacechem.0c00353
ACS Earth Space Chem. XXXX, XXX, XXX−XXX

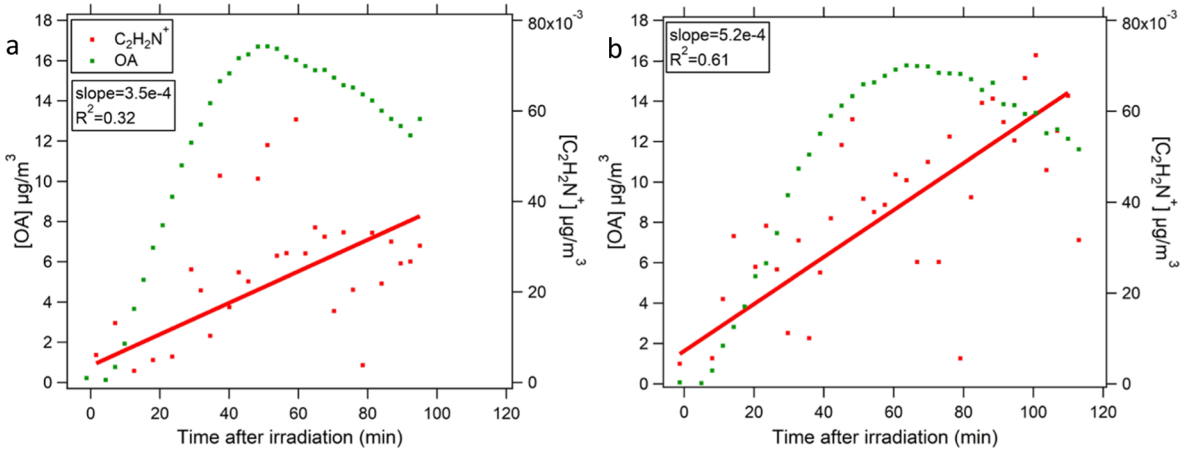

Figure 4. Time evolution of OA and $C_2H_2N^+$ concentration ($\mu g\ m^{-3}$) from mAMS from (a) 1-MN high-NO_x high-NH_3 dry experiment and (b) 1-MN high-NO_x high-NH_3 humid experiment.

presence of NH_3 also leads to the increasing trend in MAC_{org} with the extent of oxidation.

Since previous work suggested that organonitrates and nitroorganics were significant contributors to chromophore formation in BrC,[12−15] the ratio of $NO_x^+{}_{org}$ to measured organics mass (R_{ON}) was calculated as shown in Figure 3. The calculated R_{ON} from high-NO_x experiments are higher than R_{ON} in intermediate-NO_x experiments, indicating that the presence of high NO_x concentration in the chamber significantly increased the formation of organonitrate and/or nitroorganics in SOA through RO_2 + NO/NO_2 and R + NO_2 reactions compared to the intermediate-NO_x conditions; however, their contribution decreased with reaction time. The decreasing trends suggests that during the fast nucleation and initial growth period, 1-MN and its first-generation oxidized products may quickly react with NO_x and form the less volatile $NO_x^+{}_{org}$-containing compounds that partition into the particle phase. Later on, the photooxidation reaction led to formation of more oxygen-containing products, like carbonyl and carboxylic acid, peroxides, or ester functional groups, condensing onto particles, thus the overall R_{ON} decreased while contribution of oxygenated fragments, especially carboxylic acids/peroxides/or ester (m/z = 44) increased (Figure S4). Under dry conditions, R_{ON} in NH_3-free conditions decreased from ∼18% and stabilized at ∼10%, while R_{ON} under high-NH_3 conditions decreased from 30% and reached 20% at the end of the experiment. Although organonitrates and nitroorganics formation under high-NH_3 conditions might not have reached steady state due to the relatively short experimental time, R_{ON} values under high-NH_3 conditions were higher than R_{ON} from low-NH_3 experiments at similar oxidation times. The lower VOC concentration in the high-NH_3 dry experiment (up to 3−4 times lower than NH_3-free dry experiments) could be the main reason causing this result. Previous studies showed that the extent of RO_2 + RO_2 reactions (leading to formation of hydroperoxides and other oxygenated products), RO_2 + NO/NO_2 reactions (leading to organonitrate formation), and R + NO_2 reactions (leading to nitroorganic formation) vary greatly under different NO_x regimes and with different RO_2 species.[72,73] We believe that the low VOC concentration may have reduced the relative occurrence of the RO_2 + RO_2 reactions compared to RO_2 + NO/NO_2 and R + NO_2, leading to a higher R_{ON}. Regardless of the actual value of R_{ON}, given the opposing trends of R_{ON} and MAC_{org} with respect to oxidation time, organonitrate and nitroorganic formation may not be the only factor influencing the SOA optical properties. Below we discuss two other potential contributing factors.

Unlike the observations from H_2O_2-derived OH oxidation experiments described above, a prominent increase (∼2%) of some N-containing fragments (including CHN^+, CH_4N^+, and $C_2H_2N^+$) was observed when comparing the normalized HR organic mass spectra under no-NH_3 versus high-NH_3 conditions (Figures S5 and S6), indicating that NH_3 participated in the chemistry that led to the formation of NOCs. Chen et al. also observed the enhanced concentration of some N-containing fragments from the photooxidation of gasoline in the presence of NH_3.[38] Among the ions that showed significant increase with the addition of NH_3, concentration of the fragment $C_2H_2N^+$ continuously increased during the experiment in the presence of NH_3 (Figure 4); however, this increasing trend was not observed in the absence of NH_3. This observation along with the increasing MAC_{org} suggest that in the presence of high-NO_x and high-NH_3, $C_2H_2N^+$ is a reliable marker for the formation of NOCs from the reaction between NH_3 and carbonyls that leads to increased SOA absorption at 375 nm.

Another observation that is unique under the high-NO_x conditions is related to the aromatic content of the SOA. Chen et al. and Kautzman et al. reported that phthalic acid is a major PAH photooxidation product under both low- and high-NO_x conditions, and the fragment at m/z = 76 ($C_6H_4^+$) is expected to appear as a significant ion fragment from this compound in the mAMS organic mass spectra.[30,74] Our analysis confirmed the presence of $C_6H_4^+$ in this system, and the concentration of $C_6H_4^+$ relative to total organics concentration increased significantly under high-NO_x high-NH_3 conditions, while in other experiments, this fraction remained constant (Figure S7). Based on these observations, we propose that in the presence of high-NO_x and high-NH_3, the formation of phthalic acid was promoted during the latter stages of photooxidation reaction, while under intermediate-NO_x and low-NH_3 conditions, the concentration of phthalic acid relative to measured organics was unchanged during the experiment. Additionally, Lambe et al. and Liu et al. reported that the conjugated double bonds retained in photooxidation products from aromatic precursors are potentially significant contributors to the formation of chromophore in the resulting SOA.[10,27] Given the different

https://doi.org/10.1021/acsearthspacechem.0c00353
ACS Earth Space Chem. XXXX, XXX, XXX−XXX

trends but similar final values of $C_6H_4^+$ fraction from different experiments (Figure S7), we propose that although $C_6H_4^+$-containing conjugated double bonds may have contributed to the resulting SOA's absorption, it is not the most important contributor to absorption and it did not contribute significantly to the increase of MAC_{org} with time in this system.

3.3.2. Effect of RH under High-NH_3 Conditions. Similar to H_2O_2 experimental results, SSA from high-NH_3 high-NO_x conditions under two different RHs also varied significantly considering the uncertainties in SSA (0.68−0.73 vs 0.78 for humid and dry conditions, respectively). However, the MAC_{org} and k_{org} values under the different RH conditions were similar (MAC_{org} ≈ 0.69−0.70 m^2 g^{-1}, k_{org} = 0.024−0.026 under humid conditions; MAC_{org} ≈ 0.67 m^2 g^{-1}, k_{org} = 0.020 under dry conditions). One possible explanation for the apparent difference in the SSA versus MAC_{org} (or k_{org}) trends with RH is the influence of the purely scattering inorganic components of the aerosols. The fraction of purely scattering inorganic compounds was higher under dry conditions (20%) than humid conditions (5%); thus, the scattering inorganic compounds "diluted" the effect of the absorbing organic compounds, leading to a higher SSA under dry conditions. However, when the contribution of the inorganic components was taken into account and MAC_{org} and k_{org} were calculated, similar MAC_{org} and k_{org} values were determined under different RH conditions.

Hydrolysis is an important pathway for losses of organonitrate in SOA. Our results showed a significantly lower R_{ON} under humid conditions compared to dry runs (Figure 3). This is consistent with the findings by Liu et al., where 50% RH in the chamber was found to significantly decrease fractional contribution of organonitrates to OA relative to drier conditions, although hydrolysis lifetime of organonitrate species in 1-MN SOA of the current study may be different from that of 1,2,4-trimethylbenzene SOA that Liu et al. studied.[13] Our optical measurement and composition analysis show that $NO_x^+$$_{org}$-containing compounds alone did not control the optical properties of organic compounds in aerosols under different RHs here.

Similar to the results from dry, high-NH_3, high-NO_x experiments, our mAMS HR analysis from humid experiments in the presence of NH_3 also show the formation of ions corresponding to NOCs, and the concentration of $[C_2H_2N^+]$ increased as the experiments went on (Figure 4b). In general, $[C_2H_2N^+]$ in humid experiments was higher than in dry experiments, and the mass ratio of $C_2H_2N^+$ to organics under humid conditions was double the fraction under dry conditions toward the end of the experiment (0.5 vs 0.2%). Moreover, the rate of $C_2H_2N^+$ production was faster under higher humidity (~32.4 ng m^{-3} s^{-1}) compared to low-humidity runs (~20.4 ng m^{-3} s^{-1}), indicating that in the presence of water vapor, NH_3−carbonyl reactions may have produced the imines at a faster rate. One possible explanation for this observation is that the carbonyl−ammonia reactions could have occurred more efficiently in aqueous phase under higher RH.[3,32,33,44,75] Alternatively, increased RH could have suppressed aldol condensation reactions,[39,41,76] leading to higher concentrations of gas-phase carbonyl compounds and therefore a higher potential for imine formation. Considering the similar MAC_{org} values but different chemical characteristics (R_{ON} and NOCs) between dry and humid conditions (both at high-NO_x, high-NH_3), we can infer that the lower contribution from ON to total OA absorption under humid conditions was balanced out by the higher contribution from NOC to total OA under humid conditions. These findings and comparisons illustrate that we can relate $C_2H_2N^+$ concentrations with MAC_{org} in this system and confirm that $C_2H_2N^+$ is a valid marker for chromophoric NOCs in such systems. However, the overall absorption of OA in this system was determined by both ON and NOC in aerosols.

Similar to high-NO_x dry experiments, under humid conditions, we also observed the increasing trend of the fraction of $[C_6H_4^+]$ with photooxidation reaction time (Figure S7). The increasing rate and final fraction of $[C_6H_4^+]$ under humid conditions are similar to those observed under dry high-NO_x high-NH_3 conditions, indicating that humidity did not influence the formation of phthalic acid or $C_6H_4^+$-containing species in the SOA of this system.

4. CONCLUSIONS AND ATMOSPHERIC IMPLICATIONS

This study provides new insights into the formation of secondary BrC involving photooxidation reaction products of a biogenic and an aromatic hydrocarbon and NH_3. The formation of secondary BrC in the atmosphere is significant for it may potentially increase the current estimates of radiative forcing by SOA,[77,78] thus changing our understanding of the relationships between aerosols and climate change. The knowledge of secondary BrC formation in ambient environment is limited. Significant increases in MAC_{org} (and k_{org}) of 1-MN SOA formed in the presence of NH_3 to values close to those of ambient biomass burning aerosol (~0.1−0.7 m^2 g^{-1})[3,4] indicate that without considering the presence of reduced nitrogen species (i.e., NH_3) and their effects on SOA composition, a significant bias in optical properties of secondary BrC may be introduced.

Based on our results, the presence of NH_3 contributes to formation of SOA BrC from photooxidation of a PAH. Humid conditions (~40% RH) and high concentration of NO_x in the atmosphere also increase the light absorbing ability of the resulting SOA. The most likely impacted areas by this pathway are air masses impacted by biomass burning, which typically include high concentrations of aromatic VOCs, NH_3, and NO_x close to the source.[79−85] Equally important yet understudied are urban areas where aromatic VOCs, NH_3, and NO_x are also abundant.[86,87] For example, the measured aromatic VOCs at roadsides may reach several ppbv to tens of ppbv for different species,[88,89] while the mixing ratios of NH_3 and NO_x are several ppbv to hundreds of ppbv depending on the time and location.[87,90] Future urban ambient studies focused on isolating and quantifying the contribution of NH_3-driven BrC to total BrC will be valuable. Given the high degree of fragmentation in mAMS, such studies benefit from detailed compositional analysis by soft ionization techniques similar to what has been carried out for investigating BrC in biomass burning emissions.[91]

■ ASSOCIATED CONTENT

Supporting Information

The Supporting Information is available free of charge at https://pubs.acs.org/doi/10.1021/acsearthspacechem.0c00353.

Hydroxyl radical concentration in chamber experiments; organic volume fraction calculation; experimental summary; example of particle size distribution and

https://doi.org/10.1021/acsearthspacechem.0c00353
ACS Earth Space Chem. XXXX, XXX, XXX−XXX

number concentration; example of the aerosol mass distributions (for organic and nitrate ions) from mAMS measurements; difference in normalized HR organic mass spectra between two 1-MN intermediate-NO_x experiments; time series of mass contribution of [m/z = 44] to [OA] in each experiment; difference in normalized HR organic mass spectra between two 1-MN high-NO_x experiments; example of mAMS HR fit at m/z 27, 30, and 40; and time series of the mass fraction of $C_6H_4^+$ to OA from all 1-MN experiments (PDF)

AUTHOR INFORMATION

Corresponding Author

Roya Bahreini − *Department of Environmental Sciences and Environmental Toxicology Graduate Program, University of California, Riverside, Riverside, California 92521, United States;* orcid.org/0000-0001-8292-5338; Phone: +1-951-827-4506; Email: Roya.Bahreini@ucr.edu

Authors

Yumeng Cui − *Department of Environmental Sciences, University of California, Riverside, Riverside, California 92521, United States*

Alexander L. Frie − *Department of Environmental Sciences, University of California, Riverside, Riverside, California 92521, United States*

Justin H. Dingle − *Environmental Toxicology Graduate Program, University of California, Riverside, Riverside, California 92521, United States*

Stephen Zimmerman − *Department of Environmental Sciences, University of California, Riverside, Riverside, California 92521, United States*

Isis Frausto-Vicencio − *Department of Environmental Sciences, University of California, Riverside, Riverside, California 92521, United States*

Francesca Hopkins − *Department of Environmental Sciences, University of California, Riverside, Riverside, California 92521, United States*

Complete contact information is available at: https://pubs.acs.org/10.1021/acsearthspacechem.0c00353

Notes

The authors declare no competing financial interest.

ACKNOWLEDGMENTS

This work was supported by the National Science Foundation (AGS 1454374) and USDA NIFA Hatch accession no. 1015963 (project no. CA-R-ENS-5072-H).

REFERENCES

(1) Myhre, G.; Shindell, D.; Bréon, F.-M.; Collins, W.; Fuglestvedt, J.; Huang, J.; Koch, D.; Lamarque, J.-F.; Lee, D.; Mendoza, B.; Nakajima, T.; Robock, A.; Stephens, G.; Takemura, T.; Zhang, H. IPCC Fifth Assessment Report (AR5) Chapter 8: Anthropogenic and Natural Radiative Forcing. In *Climate Change 2013: The Physical Science Basis. Contribution of Working Group I to the Fifth Assessment Report of the Intergovernmental Panel on Climate Change*; Stocker, T. F., Qin, D., Plattner, G.-K., Tignor, M., Allen, S. K., Boschung, J., Nauels, A., Xia, Y., Bex, V., Midgley, P. M., Eds.; Cambridge University Press: Cambridge, United Kingdom and New York, NY, USA, 2013.

(2) Hallquist, M.; Wenger, J. C.; Baltensperger, U.; Rudich, Y.; Simpson, D.; Claeys, M.; Dommen, J.; Donahue, N. M.; George, C.; Goldstein, A. H.; Hamilton, J. F.; Herrmann, H.; Hoffmann, T.; Iinuma, Y.; Jang, M.; Jenkin, M. E.; Jimenez, J. L.; Kiendler-Scharr, A.; Maenhaut, W.; McFiggans, G.; Mentel, T. F.; Monod, A.; Prévôt, A. S. H.; Seinfeld, J. H.; Surratt, J. D.; Szmigielski, R.; Wildt, J. The Formation, Properties and Impact of Secondary Organic Aerosol: Current and Emerging Issues. *Atmos. Chem. Phys.* **2009**, *9*, 5155−5236.

(3) Laskin, A.; Laskin, J.; Nizkorodov, S. A. Chemistry of Atmospheric Brown Carbon. *Chem. Rev.* **2015**, *115*, 4335−4382.

(4) Moise, T.; Flores, J. M.; Rudich, Y. Optical Properties of Secondary Organic Aerosols and Their Changes by Chemical Processes. *Chem. Rev.* **2015**, *115*, 4400−4439.

(5) Yan, J.; Wang, X.; Gong, P.; Wang, C.; Cong, Z. Review of Brown Carbon Aerosols: Recent Progress and Perspectives. *Sci. Total Environ.* **2018**, *634*, 1475−1485.

(6) Andreae, M. O.; Gelencsér, A. Black Carbon or Brown Carbon? The Nature of Light-Absorbing Carbonaceous Aerosols. *Atmos. Chem. Phys.* **2006**, *6*, 3131−3148.

(7) Montoya-Aguilera, J.; Hinks, M. L.; Aiona, P. K.; Wingen, L. M.; Horne, J. R.; Zhu, S.; Dabdub, D.; Laskin, A.; Laskin, J.; Lin, P.; Nizkorodov, S. A. Reactive Uptake of Ammonia by Biogenic and Anthropogenic Organic Aerosols. *Multiphase Environmental Chemistry in the Atmosphere*; ACS Symposium Series; American Chemical Society, 2018; pp 127−147.

(8) Lin, P.; Fleming, L. T.; Nizkorodov, S. A.; Laskin, J.; Laskin, A. Comprehensive Molecular Characterization of Atmospheric Brown Carbon by High Resolution Mass Spectrometry with Electrospray and Atmospheric Pressure Photoionization. *Anal. Chem.* **2018**, *90*, 12493−12502.

(9) Wang, X.; Heald, C. L.; Liu, J.; Weber, R. J.; Campuzano-Jost, P.; Jimenez, J. L.; Schwarz, J. P.; Perring, A. E. Exploring the Observational Constraints on the Simulation of Brown Carbon. *Atmos. Chem. Phys.* **2018**, *18*, 635−653.

(10) Lambe, A. T.; Cappa, C. D.; Massoli, P.; Onasch, T. B.; Forestieri, S. D.; Martin, A. T.; Cummings, M. J.; Croasdale, D. R.; Brune, W. H.; Worsnop, D. R.; Davidovits, P. Relationship between Oxidation Level and Optical Properties of Secondary Organic Aerosol. *Environ. Sci. Technol.* **2013**, *47*, 6349−6357.

(11) Li, C.; He, Q.; Schade, J.; Passig, J.; Zimmermann, R.; Meidan, D.; Laskin, A.; Rudich, Y. Dynamic Changes in Optical and Chemical Properties of Tar Ball Aerosols by Atmospheric Photochemical Aging. *Atmos. Chem. Phys.* **2019**, *19*, 139−163.

(12) Lin, P.; Liu, J.; Shilling, J. E.; Kathmann, S. M.; Laskin, J.; Laskin, A. Molecular Characterization of Brown Carbon (BrC) Chromophores in Secondary Organic Aerosol Generated from Photo-Oxidation of Toluene. *Phys. Chem. Chem. Phys.* **2015**, *17*, 23312−23325.

(13) Liu, S.; Shilling, J. E.; Song, C.; Hiranuma, N.; Zaveri, R. A.; Russell, L. M. Hydrolysis of Organonitrate Functional Groups in Aerosol Particles. *Aerosol Sci. Technol.* **2012**, *46*, 1359−1369.

(14) Jiang, H.; Frie, A. L.; Lavi, A.; Chen, J. Y.; Zhang, H.; Bahreini, R.; Lin, Y.-H. Brown Carbon Formation from Nighttime Chemistry of Unsaturated Heterocyclic Volatile Organic Compounds. *Environ. Sci. Technol. Lett.* **2019**, *6*, 184−190.

(15) Lin, P.; Bluvshtein, N.; Rudich, Y.; Nizkorodov, S. A.; Laskin, J.; Laskin, A. Molecular Chemistry of Atmospheric Brown Carbon Inferred from a Nationwide Biomass Burning Event. *Environ. Sci. Technol.* **2017**, *51*, 11561−11570.

(16) Flores, J. M.; Washenfelder, R. A.; Adler, G.; Lee, H. J.; Segev, L.; Laskin, J.; Laskin, A.; Nizkorodov, S. A.; Brown, S. S.; Rudich, Y. Complex Refractive Indices in the Near-Ultraviolet Spectral Region of Biogenic Secondary Organic Aerosol Aged with Ammonia. *Phys. Chem. Chem. Phys.* **2014**, *16*, 10629−10642.

(17) Updyke, K. M.; Nguyen, T. B.; Nizkorodov, S. A. Formation of Brown Carbon via Reactions of Ammonia with Secondary Organic Aerosols from Biogenic and Anthropogenic Precursors. *Atmos. Environ.* **2012**, *63*, 22−31.

(18) Nguyen, T. B.; Lee, P. B.; Updyke, K. M.; Bones, D. L.; Laskin, J.; Laskin, A.; Nizkorodov, S. A. Formation of Nitrogen- and Sulfur-

Containing Light-Absorbing Compounds Accelerated by Evaporation of Water from Secondary Organic Aerosols. *J. Geophys. Res.: Atmos.* **2012**, *117*, D01207.
(19) Babar, Z. B.; Park, J.-H.; Lim, H.-J. Influence of NH3 on Secondary Organic Aerosols from the Ozonolysis and Photooxidation of α-Pinene in a Flow Reactor. *Atmos. Environ.* **2017**, *164*, 71−84.
(20) Laskin, J.; Laskin, A.; Nizkorodov, S. A.; Roach, P.; Eckert, P.; Gilles, M. K.; Wang, B.; Lee, H. J.; Hu, Q. Molecular Selectivity of Brown Carbon Chromophores. *Environ. Sci. Technol.* **2014**, *48*, 12047−12055.
(21) Li, K.; Wang, W.; Ge, M.; Li, J.; Wang, D. Optical Properties of Secondary Organic Aerosols Generated by Photooxidation of Aromatic Hydrocarbons. *Sci. Rep.* **2015**, *4*, 4922.
(22) Bluvshtein, N.; Lin, P.; Flores, J. M.; Segev, L.; Mazar, Y.; Tas, E.; Snider, G.; Weagle, C.; Brown, S. S.; Laskin, A.; Rudich, Y. Broadband Optical Properties of Biomass-Burning Aerosol and Identification of Brown Carbon Chromophores. *J. Geophys. Res.: Atmos.* **2017**, *122*, 5441−5456.
(23) Lin, Y.-H.; Budisulistiorini, S. H.; Chu, K.; Siejack, R. A.; Zhang, H.; Riva, M.; Zhang, Z.; Gold, A.; Kautzman, K. E.; Surratt, J. D. Light-Absorbing Oligomer Formation in Secondary Organic Aerosol from Reactive Uptake of Isoprene Epoxydiols. *Environ. Sci. Technol.* **2014**, *48*, 12012−12021.
(24) Zhong, M.; Jang, M. Light Absorption Coefficient Measurement of SOA Using a UV−Visible Spectrometer Connected with an Integrating Sphere. *Atmos. Environ.* **2011**, *45*, 4263−4271.
(25) Ofner, J.; Balzer, N.; Buxmann, J.; Grothe, H.; Schmitt-Kopplin, P.; Platt, U.; Zetzsch, C. Halogenation Processes of Secondary Organic Aerosol and Implications on Halogen Release Mechanisms. *Atmos. Chem. Phys.* **2012**, *12*, 5787−5806.
(26) Saleh, R.; Hennigan, C. J.; McMeeking, G. R.; Chuang, W. K.; Robinson, E. S.; Coe, H.; Donahue, N. M.; Robinson, A. L. Absorptivity of Brown Carbon in Fresh and Photo-Chemically Aged Biomass-Burning Emissions. *Atmos. Chem. Phys.* **2013**, *13*, 7683−7693.
(27) Liu, J.; Lin, P.; Laskin, A.; Laskin, J.; Kathmann, S. M.; Wise, M.; Caylor, R.; Imholt, F.; Selimovic, V.; Shilling, J. E. Optical Properties and Aging of Light-Absorbing Secondary Organic Aerosol. *Atmos. Chem. Phys.* **2016**, *16*, 12815−12827.
(28) Jacobson, M. Z. Isolating Nitrated and Aromatic Aerosols and Nitrated Aromatic Gases as Sources of Ultraviolet Light Absorption. *J. Geophys. Res.: Atmos.* **1999**, *104*, 3527−3542.
(29) Zhang, X.; Lin, Y.-H.; Surratt, J. D.; Weber, R. J. Sources, Composition and Absorption Ångström Exponent of Light-Absorbing Organic Components in Aerosol Extracts from the Los Angeles Basin. *Environ. Sci. Technol.* **2013**, *47*, 3685−3693.
(30) Chen, C.-L.; Kacarab, M.; Tang, P.; Cocker, D. R. SOA Formation from Naphthalene, 1-Methylnaphthalene, and 2-Methylnaphthalene Photooxidation. *Atmos. Environ.* **2016**, *131*, 424−433.
(31) Xie, M.; Chen, X.; Hays, M. D.; Lewandowski, M.; Offenberg, J.; Kleindienst, T. E.; Holder, A. L. Light Absorption of Secondary Organic Aerosol: Composition and Contribution of Nitroaromatic Compounds. *Environ. Sci. Technol.* **2017**, *51*, 11607−11616.
(32) Bones, D. L.; Henricksen, D. K.; Mang, S. A.; Gonsior, M.; Bateman, A. P.; Nguyen, T. B.; Cooper, W. J.; Nizkorodov, S. A. Appearance of Strong Absorbers and Fluorophores in Limonene-O3 Secondary Organic Aerosol Due to NH4+-Mediated Chemical Aging over Long Time Scales. *J. Geophys. Res.: Atmos.* **2010**, *115*, D05203.
(33) Laskin, J.; Laskin, A.; Roach, P. J.; Slysz, G. W.; Anderson, G. A.; Nizkorodov, S. A.; Bones, D. L.; Nguyen, L. Q. High-Resolution Desorption Electrospray Ionization Mass Spectrometry for Chemical Characterization of Organic Aerosols. *Anal. Chem.* **2010**, *82*, 2048−2058.
(34) Huang, M.; Xu, J.; Cai, S.; Liu, X.; Zhao, W.; Hu, C.; Gu, X.; Fang, L.; Zhang, W. Characterization of Brown Carbon Constituents of Benzene Secondary Organic Aerosol Aged with Ammonia. *J. Atmos. Chem.* **2018**, *75*, 205−218.
(35) Qi, X.; Zhu, S.; Zhu, C.; Hu, J.; Lou, S.; Xu, L.; Dong, J.; Cheng, P. Smog Chamber Study of the Effects of NOx and NH3 on the Formation of Secondary Organic Aerosols and Optical Properties from Photo-Oxidation of Toluene. *Sci. Total Environ.* **2020**, *727*, 138632.
(36) Na, K.; Song, C.; Switzer, C.; Cocker, D. R. Effect of Ammonia on Secondary Organic Aerosol Formation from α-Pinene Ozonolysis in Dry and Humid Conditions. *Environ. Sci. Technol.* **2007**, *41*, 6096−6102.
(37) Hao, L.; Kari, E.; Leskinen, A.; Worsnop, D. R.; Virtanen, A. Direct contribution of ammonia to α-pinene secondary organic aerosol formation. *Atmos. Chem. Phys.* **2020**, *20*, 14393−14405.
(38) Chen, T.; Liu, Y.; Ma, Q.; Chu, B.; Zhang, P.; Liu, C.; Liu, J.; He, H. Significant Source of Secondary Aerosol: Formation from Gasoline Evaporative Emissions in the Presence of SO2 and NH3. *Atmos. Chem. Phys.* **2019**, *19*, 8063−8081.
(39) Zhang, Q.; Xu, Y.; Jia, L. Secondary Organic Aerosol Formation from OH-Initiated Oxidation of m-Xylene: Effects of Relative Humidity on Yield and Chemical Composition. *Atmos. Chem. Phys.* **2019**, *19*, 15007−15021.
(40) Finlayson-Pitts, B. J.; Pitts, J. N. Rates and Mechanisms of Gas-Phase Reactions in Irradiated Organic − NOx−Air Mixtures. In *Chemistry of the Upper and Lower Atmosphere*; Finlayson-Pitts, B. J., Pitts, J. N., Eds.; Elsevier: San Diego, 2000; pp 179−263.
(41) Nguyen, T. B.; Roach, P. J.; Laskin, J.; Laskin, A.; Nizkorodov, S. A. Effect of Humidity on the Composition of Isoprene Photooxidation Secondary Organic Aerosol. *Atmos. Chem. Phys.* **2011**, *11*, 6931−6944.
(42) Liu, P.; Li, Y. J.; Wang, Y.; Bateman, A. P.; Zhang, Y.; Gong, Z.; Bertram, A. K.; Martin, S. T. Highly Viscous States Affect the Browning of Atmospheric Organic Particulate Matter. *ACS Cent. Sci.* **2018**, *4*, 207−215.
(43) Liu, Y.; Liggio, J.; Staebler, R.; Li, S.-M. Reactive Uptake of Ammonia to Secondary Organic Aerosols: Kinetics of Organonitrogen Formation. *Atmos. Chem. Phys.* **2015**, *15*, 13569−13584.
(44) Lian, X.; Zhang, G.; Yang, Y.; Lin, Q.; Fu, Y.; Jiang, F.; Peng, L.; Hu, X.; Chen, D.; Wang, X.; Peng, P.; Sheng, G.; Bi, X. Evidence for the Formation of Imidazole from Carbonyls and Reduced Nitrogen Species at the Individual Particle Level in the Ambient Atmosphere. *Environ. Sci. Technol. Lett.* **2021**, *8*, 9−15.
(45) Romonosky, D. E.; Li, Y.; Shiraiwa, M.; Laskin, A.; Laskin, J.; Nizkorodov, S. A. Aqueous Photochemistry of Secondary Organic Aerosol of α-Pinene and α-Humulene Oxidized with Ozone, Hydroxyl Radical, and Nitrate Radical. *J. Phys. Chem. A* **2017**, *121*, 1298−1309.
(46) Takeuchi, M.; Ng, N. L. Chemical composition and hydrolysis of organic nitrate aerosol formed from hydroxyl and nitrate radical oxidation of α-pinene and β-pinene. *Atmos. Chem. Phys.* **2019**, *19*, 12749−12766.
(47) Ng, N. L.; Chhabra, P. S.; Chan, A. W. H.; Surratt, J. D.; Kroll, J. H.; Kwan, A. J.; McCabe, D. C.; Wennberg, P. O.; Sorooshian, A.; Murphy, S. M.; Dalleska, N. F.; Flagan, R. C.; Seinfeld, J. H. Effect of NOx Level on Secondary Organic Aerosol (SOA) Formation from the Photooxidation of Terpenes. *Atmos. Chem. Phys.* **2007**, *7*, 5159−5174.
(48) Chan, A. W. H.; Kautzman, K. E.; Chhabra, P. S.; Surratt, J. D.; Chan, M. N.; Crounse, J. D.; Kürten, A.; Wennberg, P. O.; Flagan, R. C.; Seinfeld, J. H. Secondary Organic Aerosol Formation from Photooxidation of Naphthalene and Alkylnaphthalenes: Implications for Oxidation of Intermediate Volatility Organic Compounds (IVOCs). *Atmos. Chem. Phys.* **2009**, *9*, 3049−3060.
(49) Atkinson, R.; Arey, J. Gas-Phase Tropospheric Chemistry of Biogenic Volatile Organic Compounds: A Review. *Atmos. Environ.* **2003**, *37*, 197−219.
(50) Bouvier-Brown, N. C.; Goldstein, A. H.; Gilman, J. B.; Kuster, W. C.; de Gouw, J. A. In-Situ Ambient Quantification of Monoterpenes, Sesquiterpenes, and Related Oxygenated Compounds during BEARPEX 2007: Implications for Gas- and Particle-Phase Chemistry. *Atmos. Chem. Phys.* **2009**, *9*, 5505−5518.
(51) Dingle, J. H.; Zimmerman, S.; Frie, A. L.; Min, J.; Jung, H.; Bahreini, R. Complex Refractive Index, Single Scattering Albedo, and

https://doi.org/10.1021/acsearthspacechem.0c00353
ACS Earth Space Chem. XXXX, XXX, XXX−XXX

Mass Absorption Coefficient of Secondary Organic Aerosols Generated from Oxidation of Biogenic and Anthropogenic Precursors. *Aerosol Sci. Technol.* **2019**, *53*, 449−463.
(52) Canagaratna, M. R.; Jimenez, J. L.; Kroll, J. H.; Chen, Q.; Kessler, S. H.; Massoli, P.; Hildebrandt Ruiz, L.; Fortner, E.; Williams, L. R.; Wilson, K. R.; Surratt, J. D.; Donahue, N. M.; Jayne, J. T.; Worsnop, D. R. Elemental Ratio Measurements of Organic Compounds Using Aerosol Mass Spectrometry: Characterization, Improved Calibration, and Implications. *Atmos. Chem. Phys.* **2015**, *15*, 253−272.
(53) Chhabra, P. S.; Flagan, R. C.; Seinfeld, J. H. Elemental Analysis of Chamber Organic Aerosol Using an Aerodyne High-Resolution Aerosol Mass Spectrometer. *Atmos. Chem. Phys.* **2010**, *10*, 4111−4131.
(54) Sato, K.; Takami, A.; Isozaki, T.; Hikida, T.; Shimono, A.; Imamura, T. Mass Spectrometric Study of Secondary Organic Aerosol Formed from the Photo-Oxidation of Aromatic Hydrocarbons. *Atmos. Environ.* **2010**, *44*, 1080−1087.
(55) Farmer, D. K.; Matsunaga, A.; Docherty, K. S.; Surratt, J. D.; Seinfeld, J. H.; Ziemann, P. J.; Jimenez, J. L. Response of an Aerosol Mass Spectrometer to Organonitrates and Organosulfates and Implications for Atmospheric Chemistry. *Proc. Natl. Acad. Sci. U.S.A.* **2010**, *107*, 6670−6675.
(56) Langridge, J. M.; Lack, D.; Brock, C. A.; Bahreini, R.; Middlebrook, A. M.; Neuman, J. A.; Nowak, J. B.; Perring, A. E.; Schwarz, J. P.; Spackman, J. R.; Holloway, J. S.; Pollack, I. B.; Ryerson, T. B.; Roberts, J. M.; Warneke, C.; de Gouw, J. A.; Trainer, M. K.; Murphy, D. M. Evolution of Aerosol Properties Impacting Visibility and Direct Climate Forcing in an Ammonia-Rich Urban Environment. *J. Geophys. Res.: Atmos.* **2012**, *117*, D00V11.
(57) McComiskey, A.; Schwartz, S. E.; Schmid, B.; Guan, H.; Lewis, E. R.; Ricchiazzi, P.; Ogren, J. A. Direct Aerosol Forcing: Calculation from Observables and Sensitivities to Inputs. *J. Geophys. Res.: Atmos.* **2008**, *113*, D09202.
(58) Moosmüller, H.; Arnott, W. P. Particle Optics in the Rayleigh Regime. *J. Air Waste Manage. Assoc.* **2009**, *59*, 1028−1031.
(59) Bond, T. C.; Bergstrom, R. W. Light Absorption by Carbonaceous Particles: An Investigative Review. *Aerosol Sci. Technol.* **2006**, *40*, 27−67.
(60) DeCarlo, P. F.; Slowik, J. G.; Worsnop, D. R.; Davidovits, P.; Jimenez, J. L. Particle Morphology and Density Characterization by Combined Mobility and Aerodynamic Diameter Measurements. Part 1: Theory. *Aerosol Sci. Technol.* **2004**, *38*, 1185−1205.
(61) Bahreini, R.; Keywood, M. D.; Ng, N. L.; Varutbangkul, V.; Gao, S.; Flagan, R. C.; Seinfeld, J. H.; Worsnop, D. R.; Jimenez, J. L. Measurements of Secondary Organic Aerosol from Oxidation of Cycloalkenes, Terpenes, and m-Xylene Using an Aerodyne Aerosol Mass Spectrometer. *Environ. Sci. Technol.* **2005**, *39*, 5674−5688.
(62) Kim, H.; Paulson, S. E. Real Refractive Indices and Volatility of Secondary Organic Aerosol Generated from Photooxidation and Ozonolysis of Limonene, α-Pinene and Toluene. *Atmos. Chem. Phys.* **2013**, *13*, 7711−7723.
(63) Bohren, C. F.; Huffman, D. R. *Absorption and Scattering of Light by Small Particles*; Wiley, 1998.
(64) Michel Flores, J.; Bar-Or, R. Z.; Bluvshtein, N.; Abo-Riziq, A.; Kostinski, A.; Borrmann, S.; Koren, I.; Koren, I.; Rudich, Y. Absorbing Aerosols at High Relative Humidity: Linking Hygroscopic Growth to Optical Properties. *Atmos. Chem. Phys.* **2012**, *12*, 5511−5521.
(65) Varutbangkul, V.; Brechtel, F. J.; Bahreini, R.; Ng, N. L.; Keywood, M. D.; Kroll, J. H.; Flagan, R. C.; Seinfeld, J. H.; Lee, A.; Goldstein, A. H. Hygroscopicity of Secondary Organic Aerosols Formed by Oxidation of Cycloalkenes, Monoterpenes, Sesquiterpenes, and Related Compounds. *Atmos. Chem. Phys.* **2006**, *6*, 2367−2388.
(66) Fry, J. L.; Kiendler-Scharr, A.; Rollins, A. W.; Wooldridge, P. J.; Brown, S. S.; Fuchs, H.; Dubé, W.; Mensah, A.; dal Maso, M.; Tillmann, R.; Dorn, H.-P.; Brauers, T.; Cohen, R. C. Organic nitrate and secondary organic aerosol yield from NO3 oxidation of β-pinene evaluated using a gas-phase kinetics/aerosol partitioning model. *Atmos. Chem. Phys.* **2009**, *9*, 1431−1449.
(67) Xu, L.; Guo, H.; Boyd, C. M.; Klein, M.; Bougiatioti, A.; Cerully, K. M.; Hite, J. R.; Isaacman-VanWertz, G.; Kreisberg, N. M.; Knote, C.; Olson, K.; Koss, A.; Goldstein, A. H.; Hering, S. V.; de Gouw, J.; Baumann, K.; Lee, S.-H.; Nenes, A.; Weber, R. J.; Ng, N. L. Effects of Anthropogenic Emissions on Aerosol Formation from Isoprene and Monoterpenes in the Southeastern United States. *Proc. Natl. Acad. Sci. U.S.A.* **2015**, *112*, 37−42.
(68) Wang, L.; Atkinson, R.; Arey, J. Dicarbonyl Products of the OH Radical-Initiated Reactions of Naphthalene and the C1- and C2-Alkylnaphthalenes. *Environ. Sci. Technol.* **2007**, *41*, 2803−2810.
(69) Li, Z.; Nizkorodov, S. A.; Chen, H.; Lu, X.; Yang, X.; Chen, J. Nitrogen-Containing Secondary Organic Aerosol Formation by Acrolein Reaction with Ammonia/Ammonium. *Atmos. Chem. Phys.* **2019**, *19*, 1343−1356.
(70) Zhao, D.; Schmitt, S. H.; Wang, M.; Acir, I.-H.; Tillmann, R.; Tan, Z.; Novelli, A.; Fuchs, H.; Pullinen, I.; Wegener, R.; Rohrer, F.; Wildt, J.; Kiendler-Scharr, A.; Wahner, A.; Mentel, T. F. Effects of NOx and SO2 on the secondary organic aerosol formation from photooxidation of α-pinene and limonene. *Atmos. Chem. Phys.* **2018**, *18*, 1611−1628.
(71) Sarrafzadeh, M.; Wildt, J.; Pullinen, I.; Springer, M.; Kleist, E.; Tillmann, R.; Schmitt, S. H.; Wu, C.; Mentel, T. F.; Zhao, D.; Hastie, D. R.; Kiendler-Scharr, A. Impact of NOx and OH on secondary organic aerosol formation from β-pinene photooxidation. *Atmos. Chem. Phys.* **2016**, *16*, 11237−11248.
(72) Berndt, T.; Richters, S.; Kaethner, R.; Voigtländer, J.; Stratmann, F.; Sipilä, M.; Kulmala, M.; Herrmann, H. Gas-Phase Ozonolysis of Cycloalkenes: Formation of Highly Oxidized RO2 Radicals and Their Reactions with NO, NO2, SO2, and Other RO2 Radicals. *J. Phys. Chem. A* **2015**, *119*, 10336−10348.
(73) Sehested, J.; Christensen, L. K.; Møgelberg, T.; Nielsen, O. J.; Wallington, T. J.; Orlando, J.; Tyndall, G. S. Absolute and Relative Rate Constants for the Reactions $CH_3C(O)O_2$ + NO and $CH_3C(O)O_2$ + NO_2 and Thermal Stability of $CH_3C(O)O_2NO_2$. *J. Phys. Chem. A* **1998**, *102*, 1779−1789.
(74) Kautzman, K. E.; Surratt, J. D.; Chan, M. N.; Chan, A. W. H.; Hersey, S. P.; Chhabra, P. S.; Dalleska, N. F.; Wennberg, P. O.; Flagan, R. C.; Seinfeld, J. H. Chemical Composition of Gas- and Aerosol-Phase Products from the Photooxidation of Naphthalene. *J. Phys. Chem. A* **2010**, *114*, 913−934.
(75) Powelson, M. H.; Espelien, B. M.; Hawkins, L. N.; Galloway, M. M.; De Haan, D. O. Brown Carbon Formation by Aqueous-Phase Carbonyl Compound Reactions with Amines and Ammonium Sulfate. *Environ. Sci. Technol.* **2014**, *48*, 985−993.
(76) Hinks, M. L.; Montoya-Aguilera, J.; Ellison, L.; Lin, P.; Laskin, A.; Laskin, J.; Shiraiwa, M.; Dabdub, D.; Nizkorodov, S. A. Effect of Relative Humidity on the Composition of Secondary Organic Aerosol from the Oxidation of Toluene. *Atmos. Chem. Phys.* **2018**, *18*, 1643−1652.
(77) Ramanathan, V.; Ramana, M. V.; Roberts, G.; Kim, D.; Corrigan, C.; Chung, C.; Winker, D. Warming Trends in Asia Amplified by Brown Cloud Solar Absorption. *Nature* **2007**, *448*, 575−578.
(78) Wu, G.-M.; Cong, Z.-Y.; Kang, S.-C.; Kawamura, K.; Fu, P.-Q.; Zhang, Y.-L.; Wan, X.; Gao, S.-P.; Liu, B. Brown Carbon in the Cryosphere: Current Knowledge and Perspective. *Adv. Clim. Change Res.* **2016**, *7*, 82−89.
(79) Schauer, J. J.; Kleeman, M. J.; Cass, G. R.; Simoneit, B. R. T. Measurement of Emissions from Air Pollution Sources. 3. C1−C29 Organic Compounds from Fireplace Combustion of Wood. *Environ. Sci. Technol.* **2001**, *35*, 1716−1728.
(80) Bray, C. D.; Battye, W.; Aneja, V. P.; Tong, D. Q.; Lee, P.; Tang, Y. Ammonia Emissions from Biomass Burning in the Continental United States. *Atmos. Environ.* **2018**, *187*, 50−61.
(81) Yokelson, R. J.; Burling, I. R.; Gilman, J. B.; Warneke, C.; Stockwell, C. E.; de Gouw, J.; Akagi, S. K.; Urbanski, S. P.; Veres, P.; Roberts, J. M.; Kuster, W. C.; Reardon, J.; Griffith, D. W. T.; Johnson,

https://doi.org/10.1021/acsearthspacechem.0c00353
ACS Earth Space Chem. XXXX, XXX, XXX−XXX

T. J.; Hosseini, S.; Miller, J. W.; Cocker, D. R., III; Jung, H.; Weise, D. R. Coupling Field and Laboratory Measurements to Estimate the Emission Factors of Identified and Unidentified Trace Gases for Prescribed Fires. *Atmos. Chem. Phys.* **2013**, *13*, 89−116.
(82) Kuai, L.; Kalashnikova, O. V.; Hopkins, F. M.; Hulley, G. C.; Lee, H.; Garay, M. J.; Duren, R. M.; Worden, J. R.; Hook, S. J. Quantification of Ammonia Emissions With High Spatial Resolution Thermal Infrared Observations From the Hyperspectral Thermal Emission Spectrometer (HyTES) Airborne Instrument. *IEEE J. Sel. Top. Appl. Earth Obs. Remote Sens.* **2019**, *12*, 4798−4812.
(83) Barboni, T.; Cannac, M.; Pasqualini, V.; Simeoni, A.; Leoni, E.; Chiaramonti, N. Volatile and Semi-Volatile Organic Compounds in Smoke Exposure of Firefighters during Prescribed Burning in the Mediterranean Region. *Int. J. Wildland Fire* **2010**, *19*, 606.
(84) Navarro, K. M.; Cisneros, R.; Schweizer, D.; Chowdhary, P.; Noth, E. M.; Balmes, J. R.; Hammond, S. K. Incident Command Post Exposure to Polycyclic Aromatic Hydrocarbons and Particulate Matter during a Wildfire. *J. Occup. Environ. Hyg.* **2019**, *16*, 735−744.
(85) Wentworth, G. R.; Aklilu, Y.-a.; Landis, M. S.; Hsu, Y.-M. Impacts of a Large Boreal Wildfire on Ground Level Atmospheric Concentrations of PAHs, VOCs and Ozone. *Atmos. Environ.* **2018**, *178*, 19−30.
(86) McDonald, B. C.; de Gouw, J. A.; Gilman, J. B.; Jathar, S. H.; Akherati, A.; Cappa, C. D.; Jimenez, J. L.; Lee-Taylor, J.; Hayes, P. L.; McKeen, S. A.; Cui, Y. Y.; Kim, S.-W.; Gentner, D. R.; Isaacman-VanWertz, G.; Goldstein, A. H.; Harley, R. A.; Frost, G. J.; Roberts, J. M.; Ryerson, T. B.; Trainer, M. Volatile Chemical Products Emerging as Largest Petrochemical Source of Urban Organic Emissions. *Science* **2018**, *359*, 760−764.
(87) Elser, M.; El-Haddad, I.; Maasikmets, M.; Bozzetti, C.; Wolf, R.; Ciarelli, G.; Slowik, J. G.; Richter, R.; Teinemaa, E.; Hüglin, C.; Baltensperger, U.; Prévôt, A. S. H. High Contributions of Vehicular Emissions to Ammonia in Three European Cities Derived from Mobile Measurements. *Atmos. Environ.* **2018**, *175*, 210−220.
(88) Yuan, B.; Shao, M.; de Gouw, J.; Parrish, D. D.; Lu, S.; Wang, M.; Zeng, L.; Zhang, Q.; Song, Y.; Zhang, J.; Hu, M. Volatile Organic Compounds (VOCs) in Urban Air: How Chemistry Affects the Interpretation of Positive Matrix Factorization (PMF) Analysis. *J. Geophys. Res.: Atmos.* **2012**, *117*, D24302.
(89) Tsai, J.-H.; Lu, Y.-T.; Chung, I.-I.; Chiang, H.-L. Traffic-Related Airborne VOC Profiles Variation on Road Sites and Residential Area within a Microscale in Urban Area in Southern Taiwan. *Atmosphere* **2020**, *11*, 1015.
(90) Yang, Y.; Liu, X.; Zheng, J.; Tan, Q.; Feng, M.; Qu, Y.; An, J.; Cheng, N. Characteristics of One-Year Observation of VOCs, NOx, and O3 at an Urban Site in Wuhan, China. *J. Environ. Sci.* **2019**, *79*, 297−310.
(91) Fleming, L. T.; Lin, P.; Roberts, J. M.; Selimovic, V.; Yokelson, R.; Laskin, J.; Laskin, A.; Nizkorodov, S. A. Molecular Composition and Photochemical Lifetimes of Brown Carbon Chromophores in Biomass Burning Organic Aerosol. *Atmos. Chem. Phys.* **2020**, *20*, 1105−1129.

https://doi.org/10.1021/acsearthspacechem.0c00353
ACS Earth Space Chem. XXXX, XXX, XXX−XXX